ELSEVIER

Transport process of turbulence energy in particle-laden turbulent flow

Yohei Sato and Koichi Hishida
Department of Mechanical Engineering, Faculty of Science and Technology, Keio University, Hiyoshi, Kohoku-ku, Yokohama, Japan

The interactions between dispersed particles and fluid turbulence have been investigated experimentally and numerically in a fully developed downflow channel in water. Particle velocities and fluid velocities in the presence of 340 μm and 500 μm glass beads and 420 μm cellulose particles were measured by digital particle image velocimetry. In the presence of particles slightly greater than the Kolmogorov lengthscale of flow and with a large particle time constant, turbulence energy was augmented in the streamwise direction, which means that the energy was transported by means of particle concentration fluctuations. The dissipation rate in the equation of streamwise component of the Reynolds stress was also increased. Cellulose particles with a small particle time constant dissipated the turbulence energy in the streamwise and transverse directions due to particle drag. A multiple time-scale model in which the effect of particle concentration fluctuations on large scales of turbulent motion was reflected can present both turbulence attenuation and augmentation by particles. The particle concentration fluctuations increase the turbulence energy in the production range, which induces increasing the energy transport from the production range to the transfer range and yields finally enhancing the dissipation.

Keywords: two-phase flow; turbulence modification; multiple time-scale model

Introduction

One of the most important aspects of particle-laden turbulent flows is turbulence modification by the presence of particles. Available experimental data show the addition of small particles suppresses turbulence kinetic energy, while large particles increase turbulence. Numerous experiments of particle-laden flow (Tsuji and Morikawa 1982; Tsuji et al. 1984; Fleckhaus et al. 1987; Rogers and Eaton 1991, Kulick et al. 1994) and direct numerical simulations (DNS) of particle-laden isotropic turbulence (Squires and Eaton 1990; Elghobashi and Truesdell 1993) found that the turbulence energy was attenuated by particles smaller than the Kolmogorov lengthscale of flow and have a large particle time constant, which was mainly attributed to the extra dissipation of turbulence kinetic energy by the particles. Mechanisms of interactions between smaller particles and turbulence have thus been examined by investigating the fluid flow power spectra associated with the experiments and simulations.

With the available data as a basis, the existing particle-laden turbulence models can predict well turbulence attenuation by the particles (Elghobashi and Abou-Arab 1983; Rizk and Elghobashi 1989; Berlemont et al. 1990; Sato et al. 1996). In the most commonly used k-ε model, the particle-associated term in the equation of turbulence kinetic energy always acts as the extra dissipation due to energy consumption by particle drag (Squires and Eaton 1990). It is impossible, however, to represent an increase in the turbulence kinetic energy by these existing models. Sato et al. (1995) showed that the shortcoming of existing models was caused by modeling techniques based on one time scale, i.e., k/ε. They instead proposed a multiple time-scale model with an extra term including fluctuating particle concentration which was modeled by a gradient-diffusion hypothesis. This model has been developed by using the experimental results from a liquid–solid two-phase channel flow using a digital particle image velocimetry (Sato et al. 1995), in which the turbulence energy in low- and high-wave-number regions is increased by particle concentration fluctuations of large particles which are slightly greater than the Kolmogorov length scale of flow with regard to turbulence augmentation by particles.

The objectives of the present study are to investigate transport processes of turbulence energy between particles and fluid turbulence in a liquid–solid two-phase channel flow in water in order to understand the particle-turbulence interactions further and to develop a multiple time-scale particle-laden turbulence model accounting for the particle concentration fluctuations precisely, which has the ability to represent both turbulence attenu-

Address reprint requests to Prof. Koichi Hishida, Department of Mechanical Engineering, Faculty of Science and Technology, Keio University, 3-14-1 Hiyoshi, Kohoku-ku, Yokohama, Japan.

Received 17 October 1995; accepted 10 February 1996

Int. J. Heat and Fluid Flow 17: 202–210, 1996

655 Avenue of the Americas, New York, NY 10010

0142-727X/96/$15.00
PII S0142-727X(96)00035-X

ation and augmentation by particles. The present study shows that the present model can predict turbulence modification by the particles, which are from several fraction of to several times the Kolmogorov lengthscale of flow.

Experimental facility and techniques

The present experiments were performed in a two-dimensional (2-D), vertical downflow water channel. The channel was vertically oriented so that the gravitational force on the particles was aligned with the direction of flow. Figure 1 illustrates the basic water flow and particle supply system. The particle feeder was mounted above the entrance to the channel. The particle loading uniformity was ensured by a vibrating particle feeder which was controlled by a DC motor, and was also checked by measurements which showed the fluctuation of $\pm 8\%$ (rms value divided by mean value). Some of the properties of the flow are presented in Table 1. The Kolmogorov micro lengthscale η is calculated by direct measurements of dissipation rate of turbulence kinetic energy ε. For each set of particle conditions, the mass flow rate of water was adjusted so that the mass flow rate of the laden flow matched that of the unladen flow.

Three classes of particles were used in the present set of experiments, and their characteristics are compiled in Table 2. Particles were chosen to provide being smaller than the energy-containing scales of flow and comparable to or slightly greater

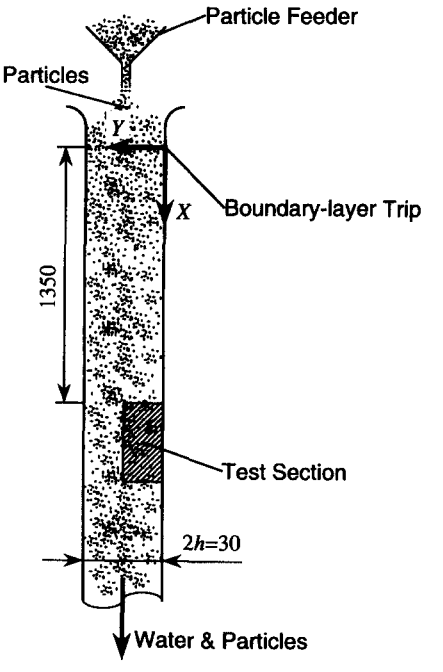

Figure 1 Schematic of water channel and particle supply system

Notation

c	fluctuating particle concentration
$\tilde{c}$	instantaneous particle concentration
$\overline{C}$	mean particle concentration
C_A	coefficient of added mass (= 0.5)
C_D	coefficient of drag
d_p	particle diameter
D_k	viscous diffusion
$E(\kappa)$	flow power spectrum
$\mathbf{g}$	gravity vector
h	channel half-width
k	turbulence kinetic energy ($= k_{PR} + k_{TR}$)
k_{PR}	turbulence kinetic energy associated with production range
k_{TR}	turbulence kinetic energy associated with transfer range
m_p	particle mass
P_k	turbulence production
Re_h, Re_{2h}	channel Reynolds number
Re_p	particle Reynolds number
Re_τ	friction-velocity Reynolds number
t	time
T_k	turbulence diffusion
u	streamwise velocity fluctuation
$\tilde{u}_{f_i}$	ith component of fluid instantaneous velocity
$\tilde{u}_{p_i}$	ith component of particle instantaneous velocity
u_τ	friction velocity
$\overline{U}$	streamwise mean velocity
$\overline{U}_{c,s}$	mean streamwise velocity of fluid at channel centerline in single-phase
$\mathbf{U}_f$	instantaneous fluid velocity vector
$\overline{u_{f_i} u_{f_i}}$	twice turbulence kinetic energy ($= 2k$)
$\overline{u_{f_i} u_{p_i}}$	fluid/particle correlation
$\mathbf{V}_p$	instantaneous particle velocity vector
V_t	particle terminal velocity ($= \tau_p g$)
$\overline{V}$	transverse mean velocity
x	streamwise direction
X	streamwise coordinate
y	transverse direction
Y	transverse coordinate

Greek

ε	dissipation rate of turbulence kinetic energy ($= \varepsilon_{TR}$)
ε_{PR}	kinetic energy transfer rate out of production range
$\varepsilon_p, \varepsilon_{p1}, \varepsilon_{p2}$	source or sink of turbulence kinetic energy by particles ($\varepsilon_p = \varepsilon_{p1} + \varepsilon_{p2}$)
η	Kolmogorov length scale
κ	wave number
ν	kinematic viscosity of air
ν_T	eddy-viscosity
Π_k, Π_ε	pressure diffusion
ρ	density
$\sigma_k, \sigma_\varepsilon$	model constants for turbulence diffusion
σ_p	standard deviation of diameter
τ_p	particle time constant
$\overline{\tau}_p^c$	mean corrected particle time constant
ϕ	particle mass loading ratio

Subscripts

f	fluid property
p	particle property

Table 1 Fluid flow parameters of a channel flow

Parameters	
Channel half-width, h	15 mm
Centerline mean velocity, $\overline{U}_{c,s}$	0.17 m/s
Channel Reynolds number, Re_{2h}	5000
Friction-Velocity Reynolds number, Re_τ	150
Estimated friction velocity, u_τ	10.1 mm/s
Kolmogorov microscale, η^*	320 μm

*Value at the channel centerline

than the Kolmogorov lengthscale of turbulence. The mean corrected particle time constant for a non-Stokesian particle in the experiments.

$$\overline{\tau_p^c} = \frac{4 d_p \rho_p}{3 \rho_f C_D \sqrt{\left(\overline{U}_p - \overline{U}_f\right)^2 + \left(\overline{V}_p - \overline{V}_f\right)^2}} \tag{1}$$

is calculated by using the drag law given by Morsi and Alexander (1972) and Clift et al. (1978).

$$C_D = \frac{29.1667}{Re_p} - \frac{3.8889}{Re_p^2} + 1.222 \qquad (1.0 < Re_p < 10.0)$$

$$C_D = \frac{24}{Re_p}(1 + 0.15\, Re_p^{0.687}) \qquad (10.0 < Re_p < 200) \tag{2}$$

where the particle Reynolds number is defined by

$$Re_p = \frac{d_p |\mathbf{V}_p - \mathbf{U}_f|}{\nu} \tag{3}$$

Velocity statistics were obtained using a digital particle image velocimetry (DPIV) developed by Sakakibara et al. (1993) which was used to measure the water flow without particles (i.e., unladen flow), the water flow in the presence of particles (i.e., laden flow), and the particles themselves. The DPIV was modified to apply to two-phase flow systems (Sato et al. 1995). A special function for two-phase flow was added to the system; i.e., detection of particle-path location within the laser sheet. When a large particle passes through the edge of the laser sheet, it is impossible to distinguish a dispersed-phase particle from a tracer of liquid. A two-control volume method comprising an Ar-laser sheet and two infrared laser diode sheets located along both sides of the Ar-laser sheet was used. The measurement uncertainty in these experiments, for a 95% confidence level, is ±2.2 mm/s for the mean velocity and ±1.7 mm/s for fluctuating velocity measurements.

Presentation and discussion of experimental results

Investigation of turbulence modification by particles requires no modification to the mean flow. Figures 2(a) and (b) depict mean streamwise velocity profiles of 500 μm glass particles and water in the presence of particles. It can be seen that the effect of particles on mean fluid is negligible, therefore, the present investigation focuses on how the turbulence is modified by the particles. The most prominent trend is that large particles augment turbulence in the core region of the channel (see Figure 8). Particle mean streamwise velocities exceeded those of the liquid phase inducing particle wake (Hishida et al. 1996), and particles were less able to respond to fluid turbulence in the streamwise and transverse directions (Sato et al. 1995).

To further examine the effect of particles on turbulence, fluid flow power spectra at the channel centerline in the streamwise and transverse directions are displayed in Figures 3 and 4, respectively. The flow power spectra in the low-wave-number region are calculated by the fast Fourier transform (FFT) of time series of velocity fluctuations at one point, at the centerline of the channel:

$$E(\kappa)_{\text{low}} = \int_0^{T\overline{U}_f} |u_f(t\overline{U}_f) e^{-i\kappa(t\overline{U}_f)}|^2 \, d(t\overline{U}_f) \tag{4}$$

where T is measuring time. While the spectra in the high-wave-number region are calculated by the Fourier transform of centerline velocities in the instantaneous measuring section:

$$E(\kappa)_{\text{high}} = \int_{x_{\min}}^{x_{\max}} |u_f(x) e^{-i\kappa x}|^2 \, dx \tag{5}$$

where $x_{\max}$ and $x_{\min}$ are the maximum and minimum values of coordinate in the streamwise direction in the test section.

It can be seen from Figure 3 that 340 and 500 μm glass particles augmented streamwise turbulence energy in both the low- and high-wave-number regions. 400 μm cellulose particles with a small particle time constant augmented the energy only in the high-wave-number region. An increase in the turbulence energy in the high-wave-number region is mainly due to particle drag, which is consistent with the experimental observations of Rogers and Eaton (1991) and Kulick et al. (1994). It can be concluded from experimental observations that the effect of particle concentration fluctuations (Sato et al. 1995 for 340 μm glass particles; Hishida et al. 1996 for 500 μm glass particles) on

Table 2 Particle properties in a channel flow

Properties	Glass	Cellulose	Glass
Number mean diameter, d_p	341.6 μm	417.7 μm	497.9 μm
SD of diameter, σ_p	22.1 μm	27.5 μm	31.0 μm
Density, ρ_p	2590 kg/m^3	1500 kg/m^3	2590 kg/m^3
Particle time constant, τ_p	19 ms	19 ms	42 ms
Corrected time constant, $\overline{\tau_p^c}$	5.0 ms	2.7 ms	7.8 ms
Terminal velocity, V_t ($=\tau_p g$)	4.9 cm/s	2.6 cm/s	7.5 cm/s
Particle mass loading ratio, ϕ	1.3×10^{-2}	2.3×10^{-3}	4.6×10^{-3}
	1.8×10^{-2}	1.3×10^{-2}	1.1×10^{-2}
	3.2×10^{-2}	2.5×10^{-2}	1.7×10^{-2}
Particle Reynolds number range, Re_p	8–12	2–14	30–40

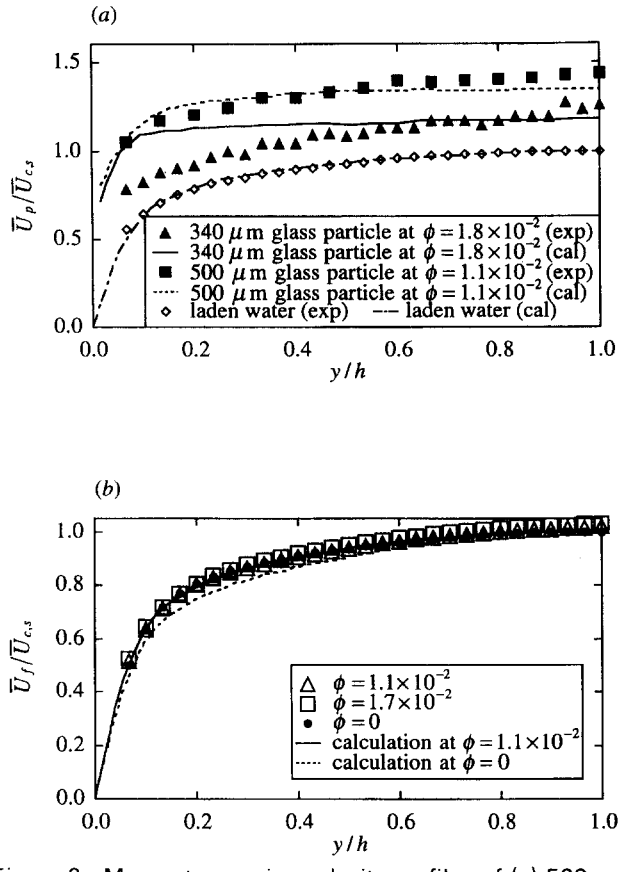

Figure 2 Mean streamwise velocity profiles of (a) 500-μm glass particles and (b) water in the presence of 500-μm glass particles

large scales of turbulent motion induced augmentation of the turbulence energy in the low-wave-number regions.

Further insight may be gained by comparing the fluid flow power spectra in the streamwise (Figure 3) and transverse directions (Figure 4). Heavy particles less responsive to high-frequency fluctuations in the transverse direction are not seen to modify the turbulence energy in the high-wave-number region. There is apparent augmentation of the transverse turbulence energy in the high-wave-number region in the presence of cellulose particles.

For further investigation of the interactions between particles and turbulence, dissipation rates in the budget of streamwise, $\overline{u_f^2}$, and transverse intensities, $\overline{v_f^2}$, are considered, which are given by

$$\varepsilon_{ij} = 2\nu\overline{\frac{\partial u_{f_i}}{\partial x_k}\frac{\partial u_{f_j}}{\partial x_k}} \tag{6}$$

Variation of dissipation rates at the channel centerline in the streamwise and transverse directions are shown in Figures 5 and 6, respectively. Although the measurement uncertainty is considerably larger than that of other turbulence quantities (included as error bars in Figures 5 and 6), it is considered to be shown in a general tendency. The dissipation rates in the streamwise direction increase as mass loading of 500 μm glass particles is increased. It can be seen from Figure 5 that the dissipation rates in the presence of 420 μm cellulose particles decrease with an increase in the mass loading. 500 μm glass particles augmented the turbulence energy due to a large inertia (Figure 3c), which yields an increase in the dissipation rate in the streamwise direction (Figure 5), however, there is no effect on the transverse dissipation rate (Figure 6).

It can be concluded that particles slightly greater than the Kolmogorov lengthscale and have a large particle time constant augmented turbulence, whereby energy is transported by the particle concentration fluctuations, yielding an increase in the dissipation of turbulence energy in the streamwise direction. Because there is no change in the transverse dissipation rate, the direct influence of larger particles on turbulence is prominent in the streamwise direction due to particle inertia. The effect of particles with a small particle time constant on turbulence is mainly attributed to the particle drag, which identifies an increase in the turbulence energy in the high-wave-number region, in both directions and a decrease in the dissipation of turbulence kinetic energy.

Overview of the simulation

Multiple time-scale model for particle-laden turbulent flows

Sato et al. (1995) have established a multiple time-scale particle-laden turbulence model with the ability to represent turbulence modification by the presence of particles; i.e., turbulence attenu-

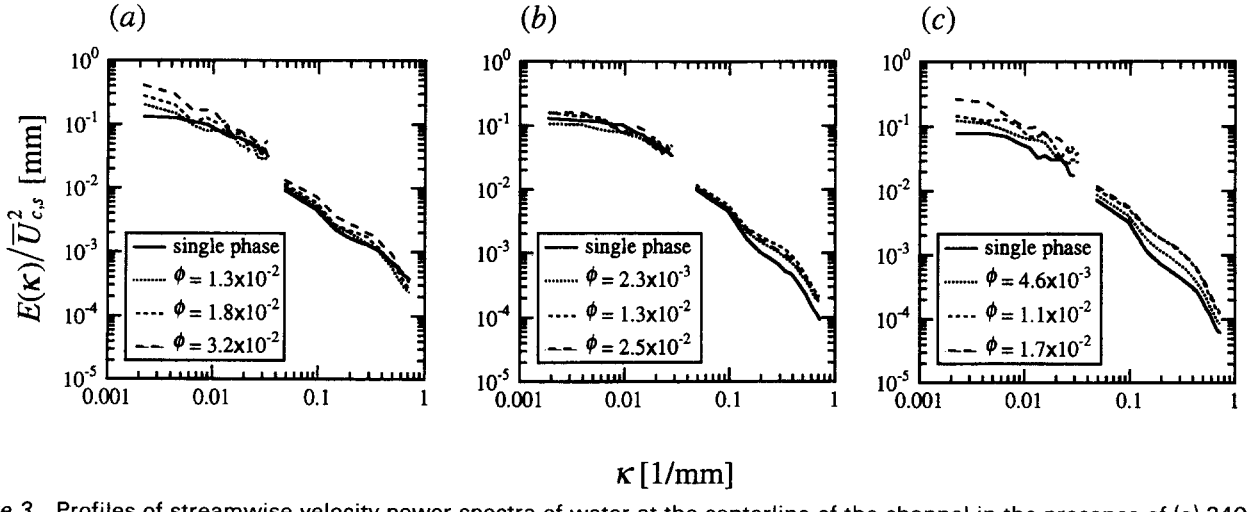

Figure 3 Profiles of streamwise velocity power spectra of water at the centerline of the channel in the presence of (a) 340-μm glass particles; (b) 420-μm cellulose particles; (c) 500-μm glass particles

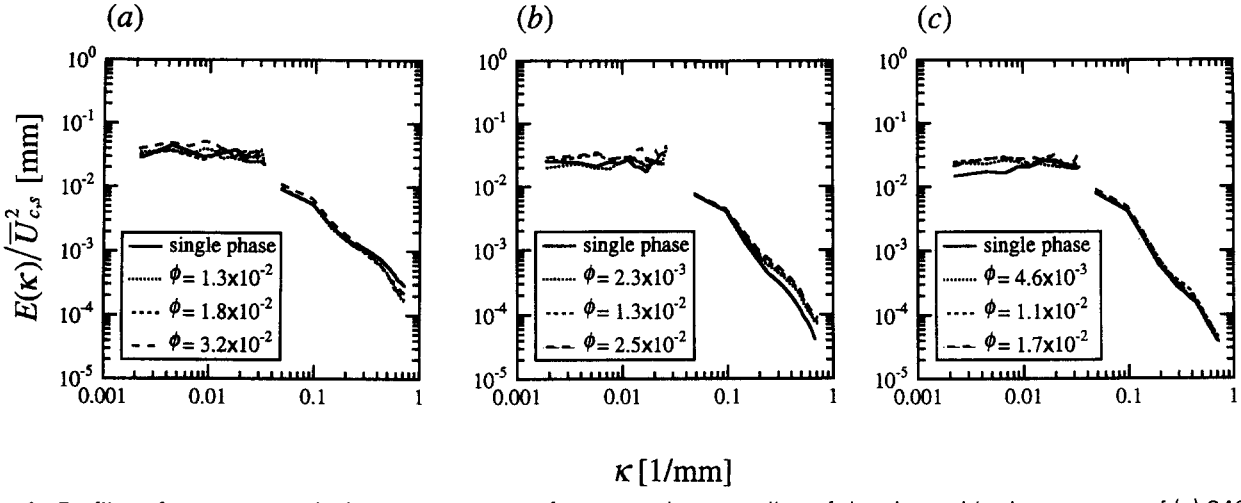

Figure 4 Profiles of transverse velocity power spectra of water at the centerline of the channel in the presence of (a) 340-μm glass particles; (b) 420-μm cellulose particles; (c) 500-μm glass particles

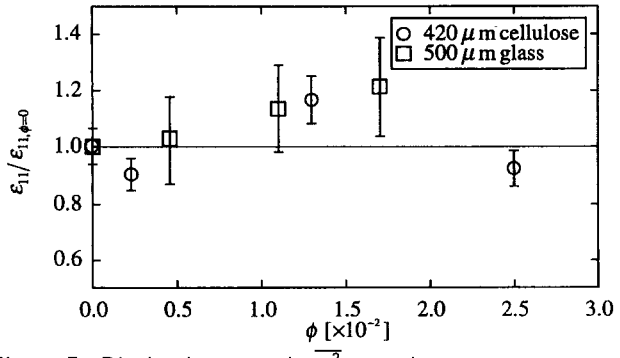

Figure 5 Dissipation rates in $\overline{u_f^2}$-equation

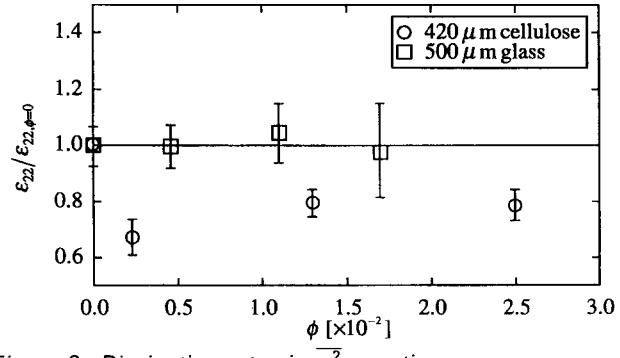

Figure 6 Dissipation rates in $\overline{v_f^2}$-equation

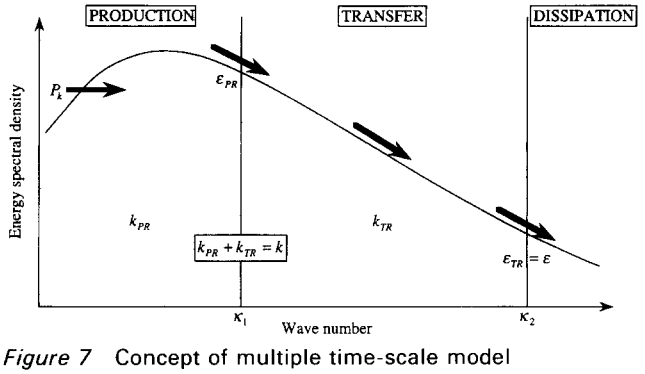

Figure 7 Concept of multiple time-scale model

ation and augmentation. Figure 7 illustrates a concept of the modeling, which divides the energy-containing part of the spectrum into two regions (Hanjalic et al. 1980; Nagano et al. 1994).

Considering the drag term in the equation of particle motion, the mean corrected particle time constant, $\overline{\tau}_p^c$, is defined as

$$\overline{\tau}_p^c = 1 \Big/ \left(\frac{3}{4} \frac{C_D}{d_p} \frac{\rho_f}{\rho_p} \left| \overline{\mathbf{V}}_p - \overline{U}_f \right| \right) \tag{7}$$

The drag force in the Navier–Stokes equation can be written as

$$\text{drag force} \approx -\frac{1}{\overline{\tau}_p^c}(\tilde{u}_{p_i} - \tilde{u}_{f_i}) \tag{8}$$

Source or sink of the turbulence kinetic energy due to momentum exchange with the particles is then

$$\varepsilon_p \approx \frac{\overline{C}}{\rho_f \overline{\tau}_p^c} \overline{u_{f_i} u_{f_i}} - \frac{\overline{C}}{\rho_f \overline{\tau}_p^c} \overline{u_{f_i} u_{p_i}} + \frac{1}{\rho_f \overline{\tau}_p^c} \left(\overline{U}_{f_i} - \overline{U}_{p_i} \right) \overline{c u_{f_i}} + \frac{1}{\rho_f \overline{\tau}_p^c} \left(\overline{c u_{f_i} u_{f_i}} - \overline{c u_{f_i} u_{p_i}} \right) \tag{9}$$

In the multiple time-scale model, the extra term ε_p in k-equation is split into the two regions; i.e., turbulence kinetic energy associated with production range k_{PR}, and transfer range k_{TR}. The first term of Equation 9 reduces to

$$\frac{\overline{C}}{\rho_f \overline{\tau}_p^c} \overline{u_{f_i} u_{f_i}} = \frac{\overline{C}}{\rho_f \overline{\tau}_p^c} 2k = \frac{\overline{C}}{\rho_f \overline{\tau}_p^c} 2k_{\mathrm{PR}} + \frac{\overline{C}}{\rho_f \overline{\tau}_p^c} 2k_{\mathrm{TR}} \tag{10}$$

In the present study, $\overline{u_{f_i} u_{p_i}}$, is evaluated by

$$\overline{u_{f_i} u_{p_i}} = \overline{\tilde{u}_{f_i} \tilde{u}_{p_i}} - \overline{U}_{f_i} \overline{U}_{p_i} \tag{11}$$

in the particle Lagrangian simulation (Berlemont et al. 1990).

Sato et al. (1995) performed modeling the third term by using a gradient-diffusion hypothesis and neglected the fourth term in Equation 9. In the present study, the third and fourth terms which include particle concentration fluctuations c are evaluated

as follows:

$$\overline{cu_{f_i}} = \overline{\tilde{c}\tilde{u}_{f_i}} - \overline{C}\,\overline{U_{f_i}} \tag{12}$$

$$\overline{cu_{f_i}u_{f_i}} = \overline{\tilde{c}\tilde{u}_{f_i}\tilde{u}_{f_i}} - \overline{C}\,\overline{U_{f_i}}^2 - \overline{C}\,\overline{u_{f_i}u_{f_i}} - 2\overline{cu_{f_i}}\,\overline{U_{f_i}} \tag{13}$$

$$\overline{cu_{f_i}u_{p_i}} = \overline{\tilde{c}\tilde{u}_{f_i}\tilde{u}_{p_i}} - \overline{C}\,\overline{U_{f_i}U_{p_i}} - \overline{C}\,\overline{u_{f_i}u_{p_i}} - \overline{cu_{f_i}}\,\overline{U_{p_i}} - \overline{cu_{p_i}}\,\overline{U_{f_i}} \tag{14}$$

where $\tilde{c}$ is the instantaneous particle concentration computed in the particle Lagrangian simulation techniques. It was observed in the experiments that particle concentration fluctuations affected the turbulence energy in the low-wave-number region, therefore, the extra terms in each region are modeled as

$$\frac{Dk_{\mathrm{PR}}}{Dt} = \frac{\partial}{\partial x_j}\left[\left(\nu + f_T\frac{\nu_T}{\sigma_k}\right)\frac{\partial k_{\mathrm{PR}}}{\partial x_j}\right] + P_k - \varepsilon_{\mathrm{PR}} - \varepsilon_{p1} \tag{15}$$

$$\frac{Dk_{\mathrm{TR}}}{Dt} = \frac{\partial}{\partial x_j}\left[\left(\nu + f_T\frac{\nu_T}{\sigma_k}\right)\frac{\partial k_{\mathrm{TR}}}{\partial x_j}\right] + \varepsilon_{\mathrm{PR}} - \varepsilon_{\mathrm{TR}} + \Pi_k - \varepsilon_{p2} \tag{16}$$

where

$$\varepsilon_{p1} = \frac{\overline{C}}{\rho_f\overline{\tau_p^c}}2k_{\mathrm{PR}} - \frac{\overline{C}}{\rho_f\overline{\tau_p^c}}\overline{u_{f_i}u_{p_i}} + \frac{1}{\rho_f\overline{\tau_p^c}}\left(\overline{U}_{f_i} - \overline{U}_{p_i}\right)\overline{cu_{f_i}} + \frac{1}{\rho_f\overline{\tau_p^c}}\left(\overline{cu_{f_i}u_{f_i}} - \overline{cu_{f_i}u_{p_i}}\right) \tag{17}$$

$$\varepsilon_{p2} = \frac{\overline{C}}{\rho_f\overline{\tau_p^c}}2k_{\mathrm{TR}} \tag{18}$$

The effect of particles on ε_{p1} and ε_{p2} are parameterized analogously to that of the destruction of dissipation term in majority of k-ε models:

$$\frac{D\varepsilon_{\mathrm{PR}}}{Dt} = \frac{\partial}{\partial x_j}\left[\left(\nu + f_T\frac{\nu_T}{\sigma_\varepsilon}\right)\frac{\partial \varepsilon_{\mathrm{PR}}}{\partial x_j}\right] + c_{\varepsilon P1}f_1\frac{\varepsilon_{\mathrm{PR}}}{k_{\mathrm{PR}}}P_k - c_{\varepsilon P2}f_2\frac{\varepsilon_{\mathrm{PR}}^2}{k_{\mathrm{PR}}} - c_{\varepsilon p1}\frac{\varepsilon_{\mathrm{PR}}}{k_{\mathrm{PR}}}\varepsilon_{p1} \tag{19}$$

$$\frac{D\varepsilon_{\mathrm{TR}}}{Dt} = \frac{\partial}{\partial x_j}\left[\left(\nu + f_T\frac{\nu_T}{\sigma_\varepsilon}\right)\frac{\partial \varepsilon_{\mathrm{TR}}}{\partial x_j}\right] + c_{\varepsilon T1}f_3\frac{\varepsilon_{\mathrm{TR}}}{k_{\mathrm{TR}}}\varepsilon_{\mathrm{PR}} - c_{\varepsilon T_2}f_4\frac{\varepsilon_{\mathrm{TR}}^2}{k_{\mathrm{TR}}} + \Pi_\varepsilon - c_{\varepsilon p2}\frac{\varepsilon_{\mathrm{TR}}}{k_{\mathrm{TR}}}\varepsilon_{p2} \tag{20}$$

where the model constants are $c_{\varepsilon p_1} = 1.2$ and $c_{\varepsilon p2} = 1.2$.

The single-phase flow model by Nagano et al. (1994) was used, and then the eddy-viscosity and model constants are

$$\nu_T = c_{\mu 1}f_{\mu 1}\frac{kk_{\mathrm{PR}}}{\varepsilon_{\mathrm{PR}}} \tag{21}$$

$$c_{\mu 1} = 0.2,\ \sigma_k = 1.3,\ \sigma_\varepsilon = 1.74,\ c_{\varepsilon P1} = 1.75,\ c_{\varepsilon P2} = 1.9,$$

$$c_{\varepsilon T1} = 1.56,\ c_{\varepsilon T2} = 1.75 \tag{22}$$

To represent the individual normal Reynolds stresses, a nonlinear model proposed by Speziale (1991) was used.

Two-way coupling simulations were performed between the Eulerian field simulation and the particle Lagrangian simulation in which the equation of particle motion reduces to (Sato et al. 1995)

$$m_p\frac{d\mathbf{V}_p}{dt} = -\frac{3}{4}\frac{m_p}{d_p}\frac{\rho_f}{\rho_p}C_D(\mathbf{V}_p - \mathbf{U}_f)|\mathbf{V}_p - \mathbf{U}_f| + m_p\left(1 - \frac{\rho_f}{\rho_p}\right)\mathbf{g} - m_p\frac{\rho_f}{\rho_p}C_A\frac{d(\mathbf{V}_p - \mathbf{U}_f)}{dt} + m_p\frac{\rho_f}{\rho_p}\frac{D\mathbf{U}_f}{Dt} \tag{23}$$

Iterations were carried out between both phases until the solutions converged.

Results and discussion of simulation

A Cartesian coordinate system (x, y) with the origin on the boundary-layer trips, at the center of the channel (Figure 1) is used for all data presentation. In most of the plots, these coordinates are normalized by the channel half-width h of 15 mm. The velocity axis is made dimensionless using centerline mean velocity of unladen water $\overline{U}_{c,s}$ of 0.17 m/s. All of the numerical results in this section were obtained by ensemble averaging over 32,768 particles in a 283×63 grid.

It is obvious from Figure 2b that mean streamwise velocities of water are not modified by particles in the present numerical simulations. Figure 8 shows profiles of streamwise turbulence intensity in the presence of 500-μm glass particles. The computational result by a single time-scale model represents turbulence attenuation, while the multiple time-scale model can predict exact behavior of turbulence augmentation. The shortcoming of the single time-scale model is in the expression of time scale characterized by amount of turbulence kinetic energy. The extra dissipation of turbulence kinetic energy in the presence of particles ε_p always acts on attenuating turbulence in the k-equation.

The multiple time-scale model proposed in this study has the ability to represent turbulence augmentation in the presence of particles comparable to or slightly greater than the Kolmogorov lengthscale of flow. To ensure validation of the present model, a gas–solid two-phase channel flow by Kulick et al. (1994) was simulated. Figure 9 depicts profiles of streamwise turbulence intensity in the presence of 70 μm copper particles which are one-half the Kolmogorov lengthscale at a mass loading ratio of 0.2. Turbulence attenuation was observed in the experiments, and the present multiple time-scale model can predict the same behavior. Computation by the single time-scale model predicts attenuation in the core region of the channel; however, it overpredicts for $0.1 < y/h < 0.7$. It can be concluded that numerical

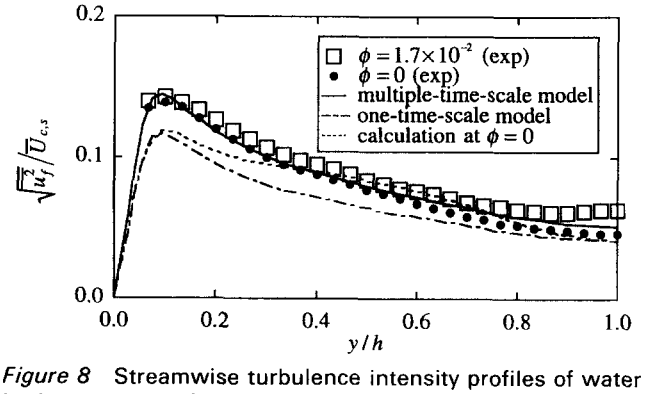

Figure 8 Streamwise turbulence intensity profiles of water in the presence of 500-μm glass particles

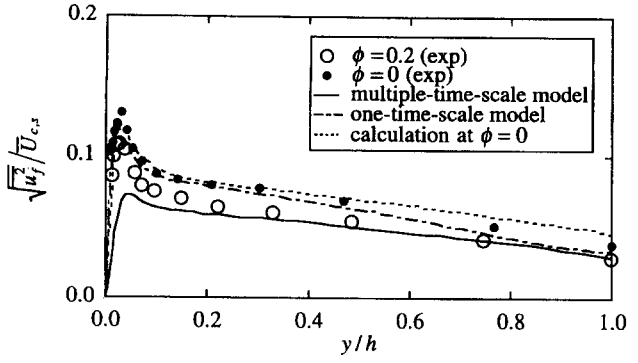

Figure 9 Streamwise turbulence intensity profiles of air in the presence of 70-μm copper particles at channel Reynolds number of 13,800 (Kulick et al. 1994)

simulations of turbulent flows laden with particles, which are from several fractions of to several times the Kolmogorov length-scale of flow, can be realized by the present multiple time-scale model.

For further investigation of the effect of particles on turbulence structure, comparison of turbulence kinetic energy budget profiles between laden and unladen flows is important. Figure 10 shows profiles of turbulence kinetic energy budget in the presence of 500-μm glass particles in comparison with those of unladen flow. The ordinate is normalized by calculated friction velocity of unladen flow. "Extra term" is calculated by difference

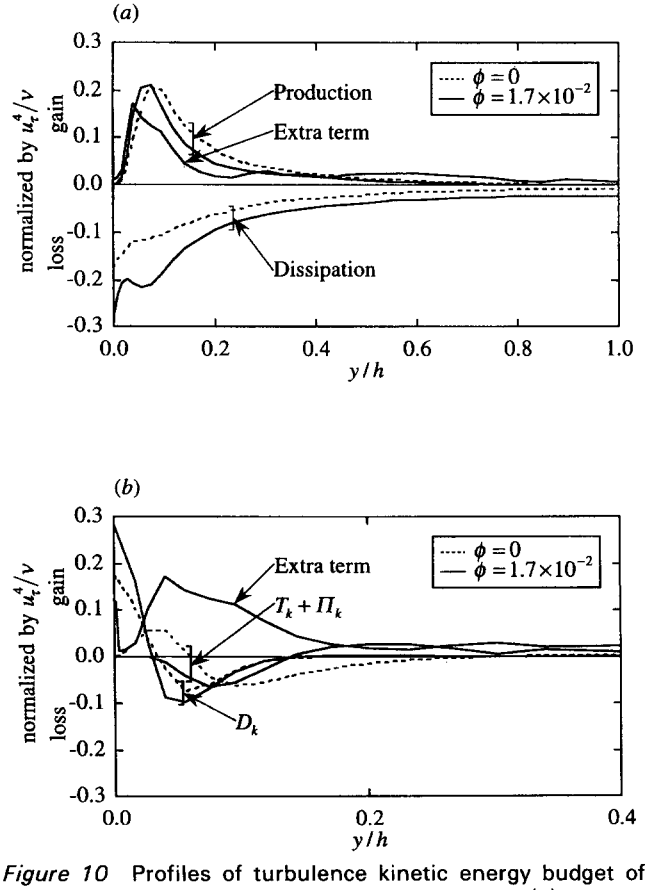

Figure 10 Profiles of turbulence kinetic energy budget of water in the presence of 500-μm glass particles: (a) balance of dominant terms; (b) balance near the wall

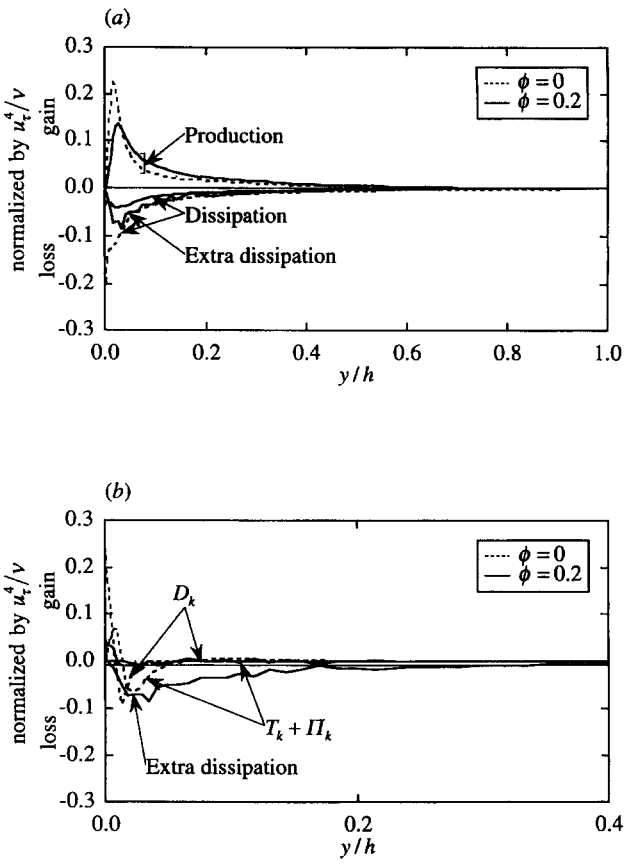

Figure 11 Profiles of turbulence kinetic energy budget of air in the presence of 70-μm copper particles at channel Reynolds number of 13,800 (Kulick et al. 1994): (a) balance of dominant terms; (b) balance near the wall

between left- and right-hand side of turbulence kinetic energy equation:

$$\text{extra term} = \left.\frac{Dk}{Dt}\right|_{\text{laden}} - (P_k + T_k + \Pi_k + D_k - \varepsilon)|_{\text{laden}} \qquad (24)$$

Turbulence augmentation by larger particles results in an increase in the dissipation rate ε rather than in the turbulence production P_k. It is observed that the "extra term" is larger than the turbulence production in the core region of the channel, which means the increase in the dissipation rate is caused mostly by the particle concentration fluctuations. The "extra term" influences the viscous diffusion D_k near the wall. It can be observed that $T_k + \Pi_k$ increases for $y/h > 0.15$.

Profiles of turbulence kinetic energy budget of air in the presence of 70-μm copper particles (Kulick et al. 1994) are exhibited in Figure 11. The turbulence production P_k and dissipation rate ε rapidly decrease near the wall due to the extra dissipation ε_p. It can be seen that the turbulence production balances with sum of the dissipation rate and the extra dissipation. The extra dissipation by particles decreases both D_k and $T_k + \Pi_k$. It can be concluded from Figures 10 and 11 that the particle concentration fluctuations affect the dissipation rate of turbulence kinetic energy when particles augment turbulence, while the extra dissipation by the particle drag alters both the turbulence production and the dissipation rate when turbulence is attenuated.

Profiles of turbulence kinetic energy in the presence of 500-μm glass particles are shown in Figure 12. It is observed that the

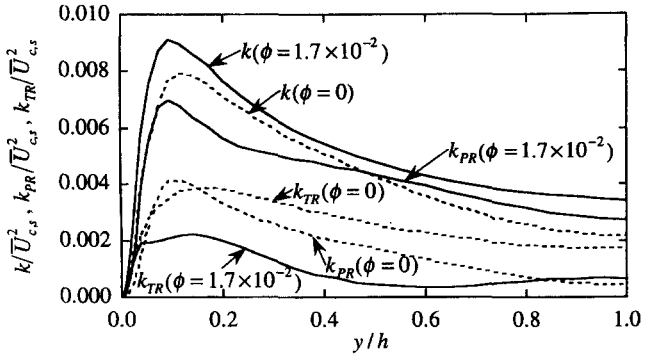

Figure 12 Profiles of turbulence kinetic energy of water in the presence of 500-μm glass particles

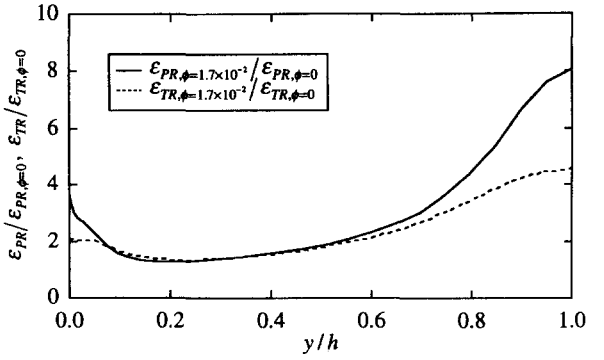

Figure 14 Profiles of transfer and dissipation rates of water in the presence of 500-μm glass particles

"total" turbulence kinetic energy k and the kinetic energy in production range k_{PR} increase, while the kinetic energy in transfer region k_{TR} decreases. These phenomena are obviously proved by the concept of the present multiple time-scale model: the particle concentration fluctuations augment the turbulence energy in the low-wave-number region, while the particle drag influences in the high-wave-number region. The present modeling is also ensured by Figure 13, which shows profiles of turbulence kinetic energy of air in the presence of 70-μm copper particles (Kulick et al. 1994). All the kinetic energies are reduced by smaller particles, due mainly to the particle drag. It can be concluded from Figures 12 and 13 that the particle concentration fluctuations increase the turbulence kinetic energy in production range, while the particle drag attenuates in transfer range.

Particles affect the turbulence energy in both production and transfer ranges, so that the kinetic energy transfer rate ε_{PR} can be changed. Figure 14 displays profiles of the ratio of ε_{PR} in the presence of particles to that of single-phase and the ratio of ε_{TR}. It is observed that the transfer ε_{PR} and dissipation rates ε_{TR} increase, especially in the core region of the channel. As the turbulence kinetic energy in the production range is increased by the particle concentration fluctuations, the transfer rate is enhanced, yielding an increase in the dissipation rate. Energy transport between production and transfer ranges is neglected in the single time-scale model, therefore models based on single time-scale are unable to predict turbulence augmentation.

Figure 15 shows profiles of ratio of transfer and dissipation rates in the presence of 70-μm copper particles (Kulick et al. 1994). Both ratios decrease, because the turbulence energy in the production range is reduced. Turbulence attenuation predicted in the present study results in decreasing the energy transport from production range to transfer range.

The multiple time-scale model established in the present study clarifies the turbulence structure of particle-laden flows by making use of important parameters; the turbulence kinetic energy in production and transfer ranges, and the kinetic energy transfer and the dissipation rates. The experimental evidence observed in the present work is reflected in modeling, therefore, the present model can contribute to understanding the particle-turbulence interactions.

Conclusions

Particle-turbulence interactions were investigated experimentally and numerically in a liquid–solid two-phase channel flow for three classes of spherical particles comparable to or greater than the Kolmogorov lengthscale of fluid turbulence. With the experimental data measured by digital particle image velocimetry, the turbulence energy in the streamwise direction was augmented in the presence of particles slightly greater than the Kolmogorov lengthscale and with a large particle time constant, which is attributed to the particle concentration fluctuations.

The dissipation rate in the budget of streamwise turbulence intensity was increased, which means an increase in the dissipation of turbulence energy. The turbulence energy was transported by means of the particle concentration fluctuations. Particles with a small particle time constant attenuated turbulence, due mainly to the particle drag, which identifies an increase in the turbulence energy in the high-wave-number region in both

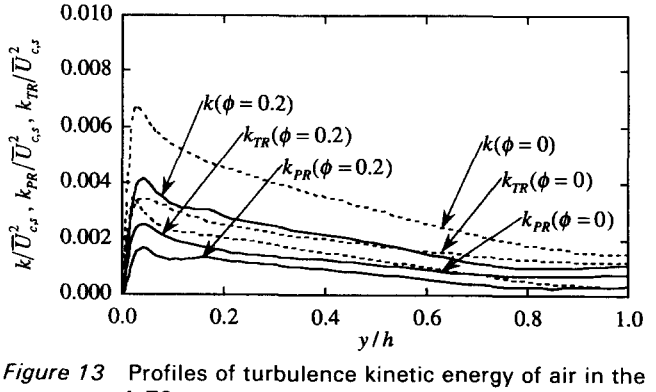

Figure 13 Profiles of turbulence kinetic energy of air in the presence of 70-μm copper particles at channel Reynolds number of 13,800 (Kulick et al. 1994)

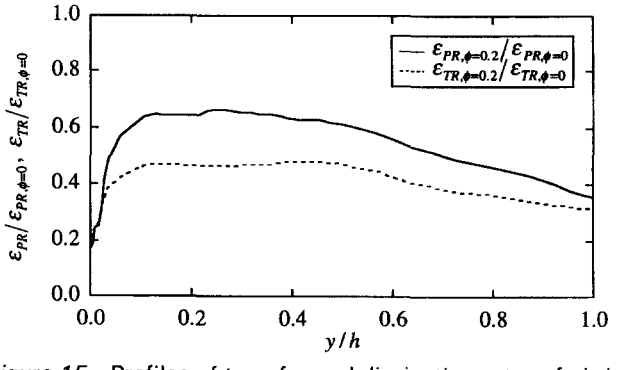

Figure 15 Profiles of transfer and dissipation rates of air in the presence of 70-μm copper particles at channel Reynolds number of 13,800 (Kulick et al. 1994)

directions and a decrease in the dissipation of turbulence kinetic energy.

The computational results showed that as the turbulence energy in production range increases, the kinetic energy transfer rate is enhanced by the particle concentration fluctuations inducing an increase in the dissipation rate of the turbulence kinetic energy. Smaller particles reduce the kinetic energy transfer rate from production range to transfer range due to the particle drag, yielding a decrease in the dissipation rate, which means turbulence is attenuated by particles smaller than the Kolmogorov lengthscale.

The multiple time-scale models for particle-laden turbulent flows proposed in the present study, which reflects the effect of the fluctuating particle concentration on turbulence, can predict turbulence modification; i.e., both turbulence attenuation and augmentation by particles.

Acknowledgments

The authors would thank A. Hanzawa and I. Hayashi for performing the experiments. This work was subsidised by the Grant-in-Aid of the Japanese Ministry of Education, Science, and Culture (grant No. 06231215).

References

Berlemont, A., Desjonquères, P. and Gouesbet, G. 1990. Particle Lagrangian simulation in turbulent flows. *Int. J. Multiphase Flow*, **16**, 19–34

Clift, R., Grace, J. R. and Weber, M. E. 1978. *Bubbles, Drops and Particles*, Academic Press, Orlando, FL

Elghobashi, S. E. and Abou-Arab, T. W. 1983. A two-equation turbulence model for two phase flows. *Phys. Fluids*, **26**, 931–938

Elghobashi, S. E. and Truesdell, G. C. 1993. On the two-way interaction between homogeneous turbulence and dispersed solid particles. I: Turbulence modification. *Phys. Fluids A*, **5**, 1790–1801

Fleckhaus, D., Hishida, K. and Maeda, M. 1987. Effect of laden solid particles on the turbulent flow structure of a round free jet. *Exp. Fluids*, **5**, 323–333

Hanjalic, K., Launder, B. E. and Schiestel, R. 1980. Multiple-time-scale concepts in turbulent transport modeling. In *Turbulent Shear Flows 2*, L. J. S. Bradbury et al. (eds.), Springer-Verlag, New York, 36–49

Hishida, K., Hanzawa, A., Sakakibara, J., Sato, Y. and Maeda, M. 1996. Turbulence structure of liquid-solid two-phase channel flow (1st report, measurements of two-phase flow by DPIV). *Trans. JSME Ser. B*, **62**, 18–25

Kulick, J. D., Fessler, J. R. and Eaton, J. K. 1994. Particle response and turbulence modification in fully developed channel flow. *J. Fluid Mech.*, **277**, 109–134

Morsi, S. A. and Alexander, A. J. 1972. An investigation of particle trajectories in two-phase flow systems. *J. Fluid Mech.*, **55**, 193–208

Nagano, Y., Kondoh, M. and Tagawa, M. 1994. Multiple-scale turbulence model for wall and free turbulent flows. *Trans. JSME Ser. B*, **60**, 1188–1195

Rizk, M. A. and Elghobashi, S. E. 1989. A two-equation turbulence model for dispersed dilute confined two-phase flows. *Int. J. Multiphase Flow*, **15**, 119–133

Rogers, C. B. and Eaton, J. K. 1991. The effect of small particles on fluid turbulence in a flat-plate, turbulent boundary layer in air. *Phys. Fluids A*, **3**, 928–937

Sakakibara, J., Hishida, K. and Maeda, M. 1993. Measurements of thermally stratified pipe flow using image-processing techniques. *Exp. Fluids*, **16**, 82–96

Sato, Y., Hanzawa, A., Hishida, K. and Maeda, M. 1995. Interactions between particle wake and turbulence in a water channel flow (PIV measurements and modelling for turbulence modification). In *Advances in Multiphase Flow 1995*, A. Serizawa et al. (eds.), Elsevier Science, New York, 27–40

Sato, Y., Hishida, K. and Maeda, M. 1996. Effect of dispersed phase on modification of turbulent flow in a wall jet. *J. Fluids Eng.*, (to be published in June)

Speziale, C. G. 1991. Analytical methods for the development of Reynolds-stress closures in turbulence. *Ann. Rev. Fluid Mech.*, **23**, 107–157

Squires, K. D. and Eaton, J. K. 1990. Particle response and turbulence modification in isotropic turbulence. *Phys. Fluids A*, **2**, 1191–1203

Tsuji, Y. and Morikawa, Y. 1982. LDV measurements of an air-solids two-phase flow in a horizontal pipe. *J. Fluid Mech.*, **120**, 385–409

Tsuji, Y., Morikawa, Y. and Shiomi, H. 1984. LDV measurements of an air-solids two-phase flow in a vertical pipe. *J. Fluid Mech.*, **139**, 417–434